ANL-SMR-2

Test Matrix for the Fundamental Sodium-CO_2 Interaction Experiment (SNAKE)

Nuclear Engineering Division

About Argonne National Laboratory

Argonne is a U.S. Department of Energy laboratory managed by UChicago Argonne, LLC under contract DE-AC02-06CH11357. The Laboratory's main facility is outside Chicago, at 9700 South Cass Avenue, Argonne, Illinois 60439. For information about Argonne and its pioneering science and technology programs, see www.anl.gov.

ANL-SMR-2

Test Matrix for the Fundamental Sodium-CO_2 Interaction Experiment SNAKE

Craig Gerardi, James J. Sienicki, Anton Moisseytsev, Mitchell T. Farmer, and Christopher Grandy
Nuclear Engineering Division
Argonne National Laboratory

April 30, 2013

ABSTRACT

An initial test matrix for fundamental sodium (Na)-carbon dioxide (CO_2) interactions has been formulated. These tests are designed to provide the data needed to understand sodium-CO_2 interactions and their consequences for Sodium-Cooled Fast Reactors (SFRs) incorporating supercritical CO_2 Brayton cycle power converters with compact diffusion-bonded sodium-to-CO_2 heat exchangers. The approach begins by considering the scenario and conditions of failure and release of CO_2 into sodium in a compact diffusion-bonded sodium-to-CO_2 heat exchanger. Phenomena following failure are identified and assessed through first principles analyses to identify the relevant regimes and conditions for which data on sodium-CO_2 interactions is needed. This is an important point because most data on sodium-CO_2 interactions reported in the literature are for conditions of less relevance to the case of a compact diffusion-bonded heat exchanger in the intermediate sodium circuit of a SFR. Based upon the results of the phenomena identification and first principles assessment, needs for fundamental experiments on sodium-CO_2 interactions are identified, and for each type of experiment, a general test matrix is formulated for testing in the ANL Na-CO_2 Interaction facility, SNAKE (S-CO_2 Na Kinetics Experiment), and other experiment facilities. An assessment of the sodium-CO_2 interaction phenomena involved in failure of compact diffusion-bonded heat exchangers and the needs for fundamental sodium-CO_2 interaction data under realistic conditions informed by such an assessment has never been carried out prior to the present report.

A condensed overview of the proposed test matrix for the SNAKE facility is shown in Table 1. The total number of experiments (including water tests) proposed is 107, with 71 of them being sodium tests. This is a very ambitious proposal especially considering that each sodium test could take approximately 2-3 weeks including preparations, nozzle change-out, and cleaning. The detailed test matrix recognizes that with the ongoing incorporation of improvements to the facility in FY 2013, testing in SNAKE in FY 2013 and early FY 2014 may largely be characterized as shakedown testing, such that testing will need to be extended into following years. These improvements and the data obtained as experiments are carried out may result in experiments being added or removed from the test matrix in order to maximize understanding of the Na-CO_2 interactions constrained by availability of resources.

A summary of the target conditions for the first thirteen experiments are also reported. All of these tests will be direct injection of CO_2 into a static sodium pool. For the first few tests, the sodium will be maintained at the lowest temperature it can safely be maintained at without any risk of freezing, around 160-180 ˚C. Over the course of several experiments the sodium temperature will gradually be increased, but it is not anticipated to reach the maximum facility operating temperature (510 ˚C) in the initial test series. The sodium column height will be kept low initially, and gradually increased, up to a maximum of approximately 80 cm. This height can be increased after enough experiments verify that gas-holdup is not pushing sodium high enough up to spill into the cover gas exhaust line. Pressure will be gradually increased from 3 MPa up to 20 MPa. Additional shakedown tests for the sodium level detector and CO gas monitors will be completed. A gas hold-up experiment to verify modeling of how high the sodium is pushed upwards by the CO_2 will also be completed.

These first tests will take place in FY 2013 and into FY 2014. It is also expected that most of the water-based tests discussed in the general test matrix will be carried out in this same time frame.

Table 1: SNAKE test matrix (H=high/large, M=medium, L=low/small)

Water tests			
CO_2 stagnation pressure, MPa	CO_2 stagnation temperature, ˚C	Water temperature, ˚C	Configuration
H	H, L	H, L	Direct nozzle injection
M	H, L	H, L	Direct nozzle injection
L	H, L	H, L	Direct nozzle injection
H, L	H, L	H	Injection into sodium channel

CO_2 impingement on plate in air	
CO_2 stagnation pressure, MPa	CO_2 stagnation temperature & intial structure temperature, ˚C
H	H, M, L
L	H, M, L

CO_2 injection from micro-nozzle into open sodium pool			
CO_2 stagnation pressure, MPa	CO_2 stagnation temperature, ˚C	Sodium column temperature, ˚C	Sodium column height, m
H	H, M, L	H, L	H, L
M	H, M, L	H, L	H, L
L	H, M, L	H, L	H, L

CO/CO_2 mixture injection from micro-nozzle into open sodium pool			
Mixture	Nozzle size, µm	Sodium column temperature, ˚C	Sodium column height, m
0.5 CO_2 + 0.5 CO	H, L	H, L	H, L
CO	H, L	H, L	H, L

CO_2 injection from micro-nozzle into a sodium channel			
CO_2 stagnation pressure, MPa	CO_2 stagnation temperature, ˚C	Sodium column temperature, ˚C	Sodium column height, m
H	H	H	M
H	L	L	M
L	H	H	M
L	L	L	M

Long term reaction product behavior in flowing sodium		
Injected gas or solid	Nozzle size, µm	Sodium temperature, ˚C
CO_2	H, L	H, M, L
CO	H, L	H, M, L
Na_2CO_3	n/a	H, M, L

Table of Contents

LIST OF FIGURES

LIST OF TABLES

1 Introduction

The Department of Energy's Office of Nuclear Energy (DOE-NE) Small Modular Reactor (SMR) program is focused on the development of clean, affordable nuclear power. SMRs have the benefit of lower initial capital investment, scalability, and siting flexibility while also having the potential for enhanced safety and security. The Advanced SMR (AdvSMR) program contains a spectrum of experimental facilities to support R&D on advanced SMR concepts. One such experimental is the ANL Na-CO_2 Interaction facility, SNAKE (S-CO_2 Na Kinetics Experiment).

The supercritical carbon dioxide (S-CO_2) Brayton cycle, coupled with a sodium-cooled SMR, has been identified as a new and innovative energy conversion technology that could contribute to meeting the SMR objectives especially in terms of improved economics. One appealing feature of this energy conversion system is the smaller footprint that the hardware requires relative to the traditional superheated steam cycle, which is in part due to the use of Printed Circuit Heat Exchanger™ (PCHE™) or Hybrid Heat Exchanger (H2X) compact diffusion-bonded heat exchangers as the heat source heat exchanger (sodium-to-CO_2) as well as the recuperator and cooler modules. Although PCHEs have a high degree of structural integrity, the potential for leaks to develop between the sodium and CO_2 coolant channels in the secondary heat exchanger cannot be ruled out, leading to discharge of high pressure CO_2 into the secondary coolant circuit. Due to the robustness of the PCHE design, catastrophic failure leading to CO_2 jet blowdown into the intermediate sodium loop is not deemed likely. Rather, small cracks (or micro-leaks) may develop in which CO_2 will bleed into the secondary system at a relatively low rate and chemically react with the sodium.

In recognition of the anticipated failure mode for a PCHE sodium-to-CO_2 heat exchanger, an Argonne experiment program, called SNAKE, was initiated in FY 2010 (see Farmer et al., 2010; Gerardi et al. 2011; Gerardi et al. 2012a and 2012b) to investigate the reaction characteristics between sodium and CO_2 under micro-leak conditions. The goal of the SNAKE facility is to:

1. Determine the fundamental nature and extent of the chemical reactions that occur between high-pressure CO_2 issuing into liquid sodium from a micro-leak across a stainless steel pressure boundary as a function of the sodium pool temperature and inlet CO_2 flowrate,
2. Examine the potential for the micro-leak to seal itself up as a result of blockage formation from the chemical reaction byproducts of the Na-CO_2 reaction, or as a result of oxide layer buildup on the crack faces,
3. Develop one-dimensional phenomenological models for the interactions between high-pressure CO_2 issuing into liquid sodium from a micro-leak across a stainless steel pressure boundary. These models will be validated using the experiment data obtained during the completion of the previous two objectives.

An initial test matrix for fundamental sodium (Na)-carbon dioxide (CO_2) interactions has been formulated to provide the data needed to understand sodium-CO_2 interactions and their consequences for Sodium-Cooled Fast Reactors (SFRs) incorporating supercritical CO_2

Brayton cycle power converters with compact diffusion-bonded sodium-to-CO_2 heat exchangers. The approach begins by considering the scenario and conditions of failure and release of CO_2 into sodium in a compact diffusion-bonded sodium-to-CO_2 heat exchanger. Phenomena following failure are identified and assessed through first principles analyses to identify the relevant regimes and conditions for which data on sodium-CO_2 interactions is needed. This is an important point because most data on sodium-CO_2 interactions reported in the literature are for conditions of less relevance to the case of a compact diffusion-bonded heat exchanger in the intermediate sodium circuit of a SFR. Based upon the results of the phenomena identification and first principles assessment, needs for fundamental experiments on sodium-CO_2 interactions are identified, and for each type of experiment, a general test matrix is formulated for testing in the ANL Na-CO_2 Interaction facility, SNAKE (S-CO_2 Na Kinetics Experiment), and other experiment facilities. An assessment of the sodium-CO_2 interaction phenomena involved in failure of compact diffusion-bonded heat exchangers and the needs for fundamental sodium-CO_2 interaction data under realistic conditions informed by such an assessment has never been carried out prior to the present report.

The detailed test matrix recognizes that with the ongoing incorporation of improvements to the facility in FY 2013, testing in SNAKE in FY 2013 and early FY 2014 may largely be characterized as shakedown testing, such that testing will need to be extended into following years. These improvements and the data obtained as experiments are carried out may result in experiments being added or removed from the test matrix in order to maximize understanding of the Na-CO_2 interactions constrained by availability of resources.

2 First principles analysis of sodium-CO_2 interactions

According to the current understanding of sodium-carbon dioxide interactions (Gicquel et al. , 2010; Gicquel et al., 2011, Eoh et al., 2010), the reaction products include elemental carbon that can dissolve in the sodium. Thus, if a leak forms in a sodium-to-CO_2 heat exchanger enabling CO_2 to enter the intermediate sodium loop of a SFR, a portion of the CO_2 is expected to be converted to elemental carbon. The carbon in the sodium can potentially cause carburization of stainless steel, although carburization is a slow rate limited process. The question thus arises of how much carbon can enter the sodium as a result of the postulated formation of micro-leaks through the stainless steel separating the CO_2 and sodium flows in a compact diffusion-bonded heat exchanger. A simple analysis of how much carbon can enter the sodium is carried out here for postulated micro-leaks.

2.1 Sodium-carbon dioxide interactions

Gicquel et al. (2010) summarizes a current view on sodium-CO_2 interactions based upon existing data. The reactions that have been observed are divided into two regimes separated by a threshold temperature that is equal to about 500 °C. Below 500 °C, two main reactions occur,

$$Na + CO_2 \rightarrow \frac{1}{4}Na_2C_2O_4 + \frac{1}{4}CO + \frac{1}{4}Na_2CO_3 ,$$

and

$$Na + \frac{1}{4}Na_2C_2O_4 \rightarrow \frac{3}{4}Na_2O + \frac{1}{4}CO + \frac{1}{4}C .$$

The first reaction involves an induction time (i.e., a waiting time) that decreases with increasing temperature creating sodium oxalate, carbon monoxide, and sodium carbonate. The oxalate formed reacts more quickly with sodium forming sodium oxide, additional carbon monoxide, and elemental carbon. Carbon monoxide is known to react with sodium but slowly with an induction step and time that decreases with rising temperature,

$$Na + \frac{1}{2}CO \rightarrow \frac{1}{2}Na_2O + \frac{1}{2}C .$$

The kinetics of this reaction are much slower than the sodium-oxalate reaction (Gicquel et al., 2010) and so the potential exists for the monoxide to loiter in the solution for some (undetermined) length of time, possibly passing out of the system as a gas that could accumulate at high points in the secondary sodium loop. There is very little reaction of carbonate with sodium. Thus, for each mole of CO_2 that enters the sodium, ¼ (to ¾) mole of C is created.

When reviewing a perspective on sodium-CO_2 reactions such as that presented Gicquel et al., (2010), it must be remembered that it is based upon sodium-CO_2 interaction experiments. A key feature of such experiments is that they do not encompass long times during which reaction products such as CO or carbonate can continue to interact with sodium. This is a fundamentally different situation from an intermediate sodium loop of a SFR. In a SFR intermediate loop, CO in the form of bubbles entrained in the sodium flow can circulate through the loop providing lengthy times for the CO and sodium to react. Similarly, small particles of sodium carbonate that form can be entrained in the sodium flow providing long times for the carbonate to react with sodium.

Above 500 °C, there is a rapid reaction between CO_2 and sodium,

$$\frac{4}{3}Na + CO_2 \rightarrow \frac{1}{3}C + \frac{2}{3}Na_2CO_3 ,$$

that forms sodium carbonate and elemental carbon. Thus, for each mole of CO_2 entering the sodium, 1/3 mole of C is created. Both reaction products are solids; no gaseous reaction products are formed.

The perspective of Gicquel et al., (2010) is that there is very little reaction of carbonate with sodium. When sodium carbonate and sodium do react, the reaction is endothermic producing sodium oxide and additional carbon,

$$\frac{8}{3}\mathrm{Na}+\frac{2}{3}\mathrm{Na_2CO_3}\rightarrow\frac{2}{3}\mathrm{C}+2\mathrm{Na_2O}\quad.$$

As discussed above, entrainment of small particles of solid carbonate in the sodium flow of an intermediate sodium circuit can provide lengthy times for interaction. Thus, there is some potential for this reaction to occur during lengthy circulation events.

2.2 Carbon dioxide flowrates into sodium

Mass fluxes of CO_2 into sodium are calculated for critical flow using the modeling in the current version of the ANL Plant Dynamics Code that has been modified since the description in Moisseytsev and Sienicki (2006). The critical flow modeling assumes an isentropic expansion of the CO_2. For a break at the hot end of a sodium-to-CO_2 heat exchanger, a critical mass flux of 34,800 kg/(m^2·s) is calculated for CO_2 at 19.9 MPa and 472 °C. For a break at the cold end of the heat exchanger, a critical mass flux of 40,100 kg/(m^2·s) is calculated for CO_2 at 19.9 MPa and 327 °C. The greater mass flux for cooler CO_2 reflects the greater density at the lower temperature.

The calculated mass fluxes are consistent with the measurements of Anderson et al. (2009) for critical flow of S-CO_2 through long tubes. In particular, for a stagnation pressure and temperature of 10.1 MPa and 130 °C, they measured a critical mass flux of 16,000 kg/(m^2·s). For critical flow of an ideal gas through an opening, the critical mass flux scales as the stagnation pressure divided by the square root of the stagnation absolute temperature. Supercritical carbon dioxide is not an ideal gas. However, applying the scaling anyway provides an estimated critical mass flux of 25,800 kg/(m^2·s) at 19.9 MPa and 327 °C. This is significantly less than 40,100 kg/(m^2·s) but the data is for critical flow through long tubes for which the flowrate is significantly reduced by the effects of friction in the tube (Anderson et al., 2009). Thus, the calculated mass fluxes are judged to be reasonable. Experimental measurements over a range of temperatures and pressures are recommended in order to accurately predict the critical flow rates.

Two microleak configurations are postulated. The first is a single 25 μm circular hole leak with CO_2 at 19.9 MPa and 327 °C. This hole size is well below the current minimum machinable hole size for SNAKE (approximately 63 μm) but puts a lower bound on the expected flow rates. The flow area is 4.91×10^{-10} m^2 and the CO_2 micro-leak flowrate is 1.97×10^{-5} kg/s.

For comparison, a second micro-leak configuration is investigated assumed to be a 113 µm circular hole which is on the upper end of the hole size that can be investigated using SNAKE due to gas flow rate measurement and safety considerations. The flow area of 1.00×10^{-8} m^2 and corresponding CO_2 micro-leak flowrate of 4.01×10^{-4} kg/s puts an upper bound on the experiment conditions possible using SNAKE. The rationale for this second configuration is that the flow area is equivalent to an assumed microcrack with a 10 µm gap and 1 mm width which might be envisioned for a compact diffusion-bonded heat exchanger.

It is assumed that ¼ of the C atoms in CO_2 that enters the sodium are transformed to elemental carbon following the chemical reactions between CO_2 and sodium. Carbon is a fraction, 0.273, of the mass of CO_2. Thus, the elemental carbon mass entering the sodium is assumed to be a fraction, 0.0682, of the mass of CO_2 entering the sodium.

2.3 Carbon solubility in sodium

Given the mass flowrate of CO_2 into the sodium and the fraction of CO_2 that is converted into C, the accumulation of carbon in the sodium can be calculated. As a figure of merit, the cumulative mass of carbon is compared with the carbon mass corresponding to the solubility limit at a specified temperature. The solubility of carbon in sodium in weight percent is given by (Natesan, 1983)

$$\ln C^0(\text{wt }\%) = 8.52 - \frac{13{,}740}{T(K)}.$$

2.4 Carbon accumulation in representative SFRs

In order to estimate carbon accumulation and carburization in a SFR, the 100 MWe AFR-100 SFR was chosen as an SMR reference design. This SFR has two intermediate sodium loops. The mass of sodium in each loop is obtained from a SAS4A/SASSYS-1 model of the AFR-100. The mass is equal to 11,100 kg. This value was checked with hand calculations using CAD drawings for a 100 MWe SFR estimating the sodium volumes in the piping, intermediate heat exchanger, sodium-to-CO_2 heat exchanger, and electromagnetic (EM) sodium pump. A sodium mass close to the 11,100 kg value was obtained confirming the mass.

Solubilities for carbon in sodium for the high and low intermediate loop sodium temperatures are shown in Table 2 together with the calculated times to reach the low and high temperature solubility limits assuming a CO_2 critical mass flux of 40,100 kg/(m^2·s). The solubility limit could be reached in the range of 20 minutes to 400 hours. This analysis assumed that there was no induction time for the reactions.

Table 2: Accumulation of carbon in an intermediate sodium loop of AFR-100

Micro-leak	25 µm hole	113 µm hole
Sodium Mass, kg	11,100	11,100
Intermediate Loop High Temperature, °C	528	528
Intermediate Loop Low Temperature, °C	373	373
C Solubility at High Temperature, wt %	1.78×10^{-4}	1.78×10^{-4}
C Solubility at Low Temperature, wt %	2.88×10^{-6}	2.88×10^{-6}
Soluble C Mass at High Temperature, kg	1.97	1.97
Soluble C Mass at Low Temperature, kg	0.0319	0.0319
Time to Reach Low Temperature Solubility Limit	6.58 hours	19.4 minutes
Time to Reach High Temperature Solubility Limit	407 hours	1200 minutes

A much larger plant, the 1000 MWt AFR-1000 SFR was chosen as a representative full-sized SFR. This plant has three intermediate sodium loops. The mass of sodium in each loop obtained from a SAS4A/SASSYS-1 model of the AFR-1000 is 136,000 kg. Solubilities for carbon in sodium for the high and low intermediate loop sodium temperatures are shown in Table 3 together with the calculated times to reach the low and high temperature solubility limits assuming a CO_2 critical mass flux of 40,100 kg/(m^2·s). The solubility limit could be reached in the range of 56 minutes to 76.7 days.

Table 3: Accumulation of carbon in an intermediate sodium loop of AFR-1000

Micro-leak	25 µm hole	113 µm hole
Sodium Mass, kg	136,000	136,000
Intermediate Loop High Temperature, °C	484	484
Intermediate Loop Low Temperature, °C	332	332
C Solubility at High Temperature, wt %	6.56×10^{-5}	6.56×10^{-5}
C Solubility at Low Temperature, wt %	6.84×10^{-7}	6.84×10^{-7}
Soluble C Mass at High Temperature, kg	8.90	8.90
Soluble C Mass at Low Temperature, kg	0.0927	0.0927
Time to Reach Low Temperature Solubility Limit	19.2 hours	56.4 minutes
Time to Reach High Temperature Solubility Limit	76.7 days	5420 minutes

Significant carbon masses are calculated to enter the intermediate loop sodium through the postulated micro-leaks relative to the solubility of carbon in sodium at the loop high temperature. Despite the fact that the flow areas of the single postulated micro-leaks are small, the critical flow mass flux of CO_2 into sodium is significant due to the high pressure of ≈ 20 MPa driving the critical flow of CO_2 through the micro-leaks. Self-plugging of micro-leaks could terminate entry of CO_2 into sodium. This will be examined in the Na-CO_2 Interaction Tests. Carburization is still a slow process even at concentrations exceeding the solubility limit and needs to be analyzed for the assumed carbon concentrations in the sodium indicated by the analysis.

Approaches must be identified and developed to detect the leakage of CO_2 into sodium at a low enough threshold such that the CO_2 circuit can be isolated from the heat exchanger limiting CO_2 entry into sodium. Approaches and instrumentation identified and developed for detecting CO_2 leakage must be tested and qualified for use on SFRs. Approaches must be

identified and developed for removing carbon from sodium. Approaches for removing carbon from sodium must be tested and qualified for use on SFRs.

2.5 Self-healing due to oxide layer growth on crack faces

As the CO_2 flows through a microcrack, the CO_2 will interact with the elements in the stainless steel on the opposing faces of the crack forming a growing oxide layer. For a sufficiently small microcrack gap thickness, the growing oxide layers could potentially fill the initial gap thickness occluding the microcrack channel and significantly reducing or even stopping the flowrate of CO_2 into the sodium. An analysis of whether such self-healing of a crack occurs can be carried out for the postulated microcrack using existing data on the oxidation/corrosion of stainless steel by CO_2.

Oxidation/corrosion data recently reported by CEA (Rouillard et al., 2012) show little oxidation and oxide layer growth for 316L stainless steel exposed to flowing CO_2 at 550 °C and 0.1 MPa pressure. After 1000 hours of exposure, the mass gain due to oxidation is about 0.4 g/m^2 from which an oxide layer thickness of about 0.3 μm is calculated. Although the CEA results were obtained at atmospheric pressure, the oxidation weight gains are similar to those previously obtained at the Japan Atomic Energy Agency (JAEA) for 316FR stainless steel at 10 and 20 MPa pressure. JAEA did not observe an effect of pressure.

For the postulated microcracks considered here, the oxide layer thickness due to oxidation of 316 stainless steel would be relatively small over the timescales of relevance such that self-healing of the crack would not occur for micron-scale or larger cracks. However, self-plugging due to the accumulation of solid reaction products in front of the micro-leak location might still occur. The accumulation of solid reaction products has been observed in sodium-CO_2 reaction tests carried out at the Korea Atomic Energy Research Institute (KAERI) (Eoh et al., 2010).

It might be questioned how self-plugging could occur inside of a sodium channel of a compact diffusion-bonded heat exchanger in the presence of flowing sodium. However, there is a laminar boundary layer next to the stainless steel wall in which the velocity goes to zero. If small particles of reaction products are envisioned to form next to the wall, one might envision that they could plug a micro-leak and resist the frictional shear stress from the flowing sodium within the boundary layer.

3 Carbon dioxide release into sodium in a compact diffusion-bonded heat exchanger

In order to identify experiments and conditions for the Na-CO_2 interaction tests, it is necessary to first assess the phenomena and conditions expected following the formation of a micro-leak in a sodium-to-CO_2 compact diffusion-bonded heat exchanger. For this purpose, a reference sodium-to-CO_2 heat exchanger is assumed and first principles analyses of the anticipated phenomena are carried out.

3.1 Reference compact diffusion-bonded heat exchanger

Figure 1 illustrates what a cross section through a Heatric, compact, diffusion-bonded, Hybrid Heat Exchanger (H2X) (Southhall, 2009) sodium-to-CO_2 heat exchanger might look like. The H2X has Printed Circuit Heat Exchanger™ (PCHE™)-type zigzagged semicircular channels on the CO_2 side and larger Formed Plate Heat Exchanger (FPHE)-type straight rectilinear channels on the sodium side. The PCHE semicircular channels are created by chemical etching of stainless steel plates while the FPHE rectilinear channels are formed through mechanical deformation of stainless steel plates. For a sodium-to-CO_2 HX, the rectilinear sodium channels might be 4 mm wide by 6 mm high with the expectation that for a size this large inadvertent plugging of the sodium channels due the precipitation of oxygen dissolved in the sodium during a postulated event would take a sufficiently long time such that plugging is unlikely or the occurrence of plugging could be detected with sufficient time to take action to prevent significant plugging of sodium channels. The larger sodium channel dimensions of a H2X relative to a PCHE are a major benefit of the H2X making it an attractive choice for a sodium-to-CO_2 HX. The various stainless steel plates are stacked together and diffusion bonded to form a core. Figure 2 shows a loose stack of stainless steel plates for a FPHE core. A "land" of solid stainless steel surrounds the CO_2 and sodium channels in the central region of the core of a diffusion-bonded HX be it a PCHE, FPHE, or H2X.

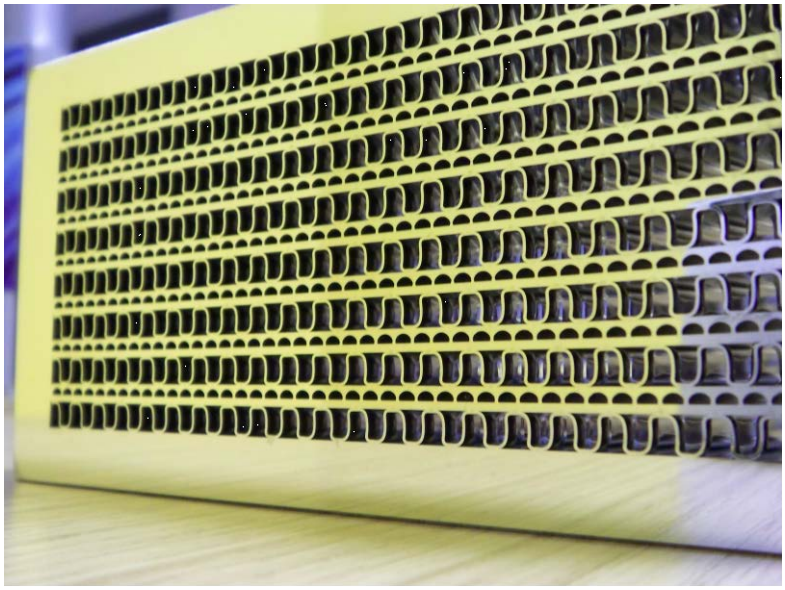

Figure 1: Example Na-to-CO_2 Hybrid Heat Exchanger (H2X) with larger formed plate heat exchanger (FPHE) cannels on the sodium side and printed circuit heat exchanger™ (PCHE™) channels on the CO_2 Side (Heatric Division of Meggitt (UK) Ltd.).

Figure 2: Stacking of stainless steel plates for formed plate heat exchanger (FPHE) core (Heatric Division of Meggitt (UK) Ltd.).

An ANL thermal hydraulics model for a H2X predicting the H2X heat transfer and pressure drop performance does not yet exist. However, the ANL PCHE model incorporated in the ANL Plant Dynamics Code for the S-CO_2 Brayton cycle (Moisseytsev and Sienicki, 2006; Moisseytsev et al., 2010) can be applied to roughly approximate H2X thermal hydraulic conditions by selecting the PCHE semicircular diameter on the sodium side to have a hydraulic diameter identical to that of a H2X 4 mm by 6 mm rectilinear sodium channel. Strictly speaking, the ANL PCHE model approximates the performance of a Heatric PCHE.

A sodium-to-CO_2 HX preconceptual design was developed for a metallic-fueled 388 MWe (1000 MWt) SFR (an earlier version of the AFR-1000) having a nominal core outlet temperature of 510 ˚C. The preconceptual design of the HX is optimized to incorporate a number of individual compact diffusion-bonded HX cores that contribute to a high S-CO_2 Brayton cycle and net plant efficiency but not so large in number as to make the sodium-to-CO_2 HX capital cost excessive. The resulting S-CO_2 Brayton cycle efficiency is 40.8 % but electrical power requirements for the sodium pumps reduce the net plant efficiency to 38.8 %. The normal operating intermediate sodium temperatures at the HX inlet and outlet are 488 and 333 ˚C, respectively. The CO_2 is heated from 327 to 473 ˚C.

The sodium-to-CO_2 HX consists of 420 2.38 MWt H2X units each having a core with a length of 1.5 m, width of 0.6 m, and stack height of 0.6 m. These are the maximum dimensions of cores that Heatric can currently diffusion bond. On the sodium side, the straight semicircular channels have a width of 4 mm, height of 6 mm, and length of 1.5 m. The hydraulic diameter of a 7.9 mm semicircular diameter sodium channel is 4.83 mm equal to that of a rectilinear 4 mm by 6 mm channel. The total sodium flow area is 0.128 m^2. The mean velocity through a sodium channel is 0.112 m/s at the inlet (hot end) and 0.108 m/s at the outlet (cold end). The corresponding Reynolds numbers are 1892 at the inlet and 1433 at the outlet. The sodium flowrate through a single core is 12.0 kg/s. The HX incorporates zigzagged 2.0 mm semicircular channels on the CO_2 side. The pressure on the CO_2 side varies from 19.949 MPa at the CO_2 inlet to 19.105 MPa at the CO_2 outlet. The CO_2 flowrate through a single core is 13.3 kg/s.

The straight sodium channels and zigzagged semicircular CO_2 channels are assumed to be arranged in a "Z configuration." In particular, the sodium is delivered to the core by means of an inlet header at one end of the core and exits the core through an outlet header at the other end. In contrast, the CO_2 enters the core by means of a header on the side of the core near the sodium exit, changes direction inside of the core to flow generally in the opposite direction to the sodium, and changes direction to exit the core through a header on the other side near the sodium inlet. Figure 2 illustrates such a Z configuration for the case of a plate for a FPHE for which the channels are straight instead of zigzagged.

Each header is connected to either a sodium pipe or a CO_2 pipe. A sodium header would have the same dimensions as a face of the core; that is 0.6 m by 0.6 m outer dimensions. It is assumed here that each header would have a depth of about half this size or 0.3 m. Similarly, each CO_2 header would have an outer height of 0.6 m equal to that of the core and a length enveloping all of the channels in the Z configuration. It is assumed that the header depth would also be half of the height or 0.3 m.

The heat exchanger units must be oriented to facilitate efficient drainage of sodium from the intermediate loop in the event of an incident or accident such as the rupture of an intermediate sodium pipe. The sodium is drained from the intermediate loop into the sodium storage vessel for the loop to limit the amount of sodium that can spill onto the floor and burn in the compartment in which the rupture occurs. A typical time to drain the sodium from an intermediate loop would be about fifteen or twenty minutes.

To assure drainage of sodium from a compact diffusion-bonded heat exchanger unit, the unit needs to be oriented at a sloping angle. The shortest drainage time can be achieved by orienting the heat exchanger vertically. Therefore, a vertical orientation is assumed in the current analysis. The sodium is assumed to flow downward through a sodium pipe connecting to the inlet sodium header at the top of the unit, flow through the inlet sodium header, flow through the straight sodium channels of the unit, flow through the outlet sodium header at the bottom of the unit and exit downward through a sodium pipe. The CO_2 is assumed to flow horizontally through a CO_2 pipe connecting to the inlet CO_2 header on the side of the unit near the bottom, flow through the inlet CO_2 header, flow generally upward through the CO_2 channels of the unit, flow through the outlet CO_2 header on the other side of the unit near the top, and exit through a horizontal CO_2 pipe.

Each individual sodium channel is assumed to be 4 mm wide by 6 mm high such that the flow area of one sodium channel is 2.4×10^{-5} $m^2$and the hydraulic diameter is 4.8 mm. The total sodium flow area through the core is 0.128 m^2 such that there are about 5330 sodium channels. For the sodium velocity at the channel outlet, 0.108 m/s, the sodium volume flowrate is 2.592×10^{-6} m^3/s for one channel and 1.382×10^{-2} m^3/s for the heat exchanger unit.

Immediately below the core, the sodium expands into the header which suddenly provides a much larger one-dimensional flow area for the sodium. Assuming that the sodium header is 2.0 cm thick, the one-dimensional flow area immediately beneath the core is 0.3136 m^2 such

that the one-dimensional sodium velocity immediately beneath the core drops to only 0.0441 m/s. As the sodium flows downward inside of the header, the cross-sectional area decreases such that the velocity of the downward flowing sodium increases.

The required sodium pipe size connecting to each sodium header may be estimated. Assuming that the sodium velocity through the pipe is limited to 3 m/s, the pipe flow area is calculated to equal 4.608×10^{-3} m^2 for which the sodium pipe inner diameter is 0.07660 m (3.016 in). This is not quite a standard pipe size, however. Assuming the use of a 3 inch Schedule 40 pipe, the standard pipe inner diameter is 0.07793 cm (3.068 in). The sodium velocity through this slightly larger diameter pipe is calculated to equal 2.90 m/s.

Although the heat exchanger design was optimized for the AFR-1000, the same heat exchanger dimensions and sodium velocities are also assumed as an approximation for the AFR-100. A smaller number of heat exchanger units would be utilized in each intermediate sodium loop of the AFR-100 relative to the AFR-1000.

3.2 Carbon dioxide expansion following heat exchanger failure

Upon exiting the micro-leak, the CO_2 will expand down to the local pressure inside of the intermediate sodium circuit. Due to the expansion of the CO_2 from a nominal pressure of up to 20 MPa to a low pressure of the intermediate sodium circuit (nearly atmospheric), very large changes in CO_2 temperature and volume will occur. Carbon dioxide is not an ideal gas and the CO_2 properties vary greatly across this pressure differential, especially near the critical point. Because of this, the proper method of assessing the temperature reduction due to the expansion would require a meshed-iterative scheme that includes conjugate heat transfer from the stainless steel micro-crack walls and sodium pool. This approach is intended to be carried out in FY 14 and FY 15. In the meantime, first-principle analyses are carried out in an attempt to put bounds on the anticipated CO_2 temperature drop due to expansion.

3.2.1 Isentropic expansion

An approximate lower bound on the CO_2 temperature inside of the sodium channel following expansion can be obtained by assuming that the CO_2 undergoes an isentropic expansion.

Provided that the final temperature of the CO_2 is not too low, then the temperature and other CO_2 properties following an isentropic expansion can be calculated using the CO_2 state equation (Span and Wagner, 1996). In particular, for a given initial state of pressure, one can obtain the specific entropy and other CO_2 properties at the initial temperature (or over a range of temperatures). One can next obtain isobaric properties at the final pressure over a range of temperatures including the final value. For a sufficiently precise temperature increment, one can accurately determine the final temperature at which the final specific entropy matches the initial value. The triple point of CO_2 is at -56.558 °C below which solid CO_2 can exist and the state properties no longer apply.

For final states calculated from an isentropic expansion for which the temperature can go below -56.558 °C, the temperature versus specific entropy chart for CO_2 from the handbook of Reynolds (1979) is used. The chart includes lines of constant pressure from which the temperature following an isentropic expansion to a specified pressure is determined. Unfortunately, the chart does not extend to the high temperatures representative of the heat exchanger. It is still possible to use the chart knowing the initial specific entropy.

Table 4 shows the final CO_2 states and temperatures calculated following an isentropic expansion from the CO_2-side pressure of 20 MPa at the high and low heat exchanger temperatures to assumed final intermediate sodium loop pressures of 0.1 MPa. The actual sodium loop pressure would be higher than this (up to 0.5 MPa), but 0.1 MPa is an appropriate assumption for these bounding calculations and show that dramatic reductions in temperature are expected. In all cases but one, the CO_2 expands to a gaseous state. Only for the lowest initial temperature is the formation of solid CO_2 (i.e., dry ice) calculated. Even in that case, however, the mass of solid CO_2 formed is very small amounting to only 2 % or less of the CO_2 mass.

Table 4: Calculated temperatures of CO_2 following isentropic expansion through micro-leak

Reactor	AFR-100	AFR-100	AFR-1000	AFR-1000
Initial CO_2 Pressure, MPa	20	20	20	20
Initial CO_2 Temperature, °C	528	373	484	332
Initial CO_2 Specific Entropy, kJ/(kg·K)	2.7073	2.4426	2.6375	2.3623
Final CO_2 State Following Expansion to 0.1 MPa	Gas	Gas	Gas	Vapor-solid mixture with quality ≥ 0.98
Final CO_2 Temperature Following Expansion to 0.1 MPa, °C	15	-68	-8.6	-78
Temperature Reduction Following Expansion to 0.1 MPa, °C	513	441	493	410

The calculated reductions in CO_2 temperature range from 410 to 513 °C. This is the reduction in the CO_2 temperature relative to the temperature of the surrounding sodium and structure in the heat exchanger. Impingement of CO_2 from the micro-leak upon the stainless steel in the vicinity of the micro-leak as well as flow of CO_2 over stainless steel in the vicinity of the micro-leak following local voiding of the sodium channel could result in thermal shocking of the stainless steel. Extreme thermal shocking might result in the formation of additional cracks and leaks between heat exchanger channels. There are two main possibilities here. If a new crack forms between the affected sodium channel and another adjacent CO_2 channel, then additional CO_2 from that channel will enter the sodium channel. If a new crack forms between the affected sodium channel and an adjacent sodium channel, then it becomes possible for CO_2 to enter the other sodium channel. However, the pressure difference

between the two sodium channels would be low which would limit the rate at which CO_2 could enter the other sodium channel. If the CO_2 temperature drops below the freezing point of sodium, 98 °C, there is potential for the sodium to freeze and plug the channel.

3.2.2 Heat transfer to carbon dioxide in the failed channel

The final temperatures calculated above are lower bounds because an isentropic expansion is assumed. As the flowing CO_2 expands and the CO_2 temperature falls, the temperature difference between the surrounding stainless steel wall and the bulk CO_2 results in heat transfer from the stainless steel to the CO_2. If a significant amount of heat can be transferred to the CO_2, then the expansion will not be isentropic and the final temperatures will be higher than those calculated in Table 3.

The potential for convective heat transfer between the flowing CO_2 and stainless steel to add energy to the flowing CO_2 is readily assessed. The steady state temperature of a fluid flowing through a one-dimensional channel having an unvarying wall temperature is given by

$$\rho u c_p A \frac{dT}{dx} = hP\,(T_w - T)$$

where

ρ = density,
u = velocity,
c_p = specific heat,
A = flow area,
T = bulk fluid temperature,
x = distance coordinate,
h = heat transfer coefficient between wall and bulk fluid,
P = wetted perimeter,
T_w = wall temperature.

Defining the hydraulic diameter as

$$D_h = \frac{4A}{P},$$

and $y=T_w-T$, the equation reduces to

$$\frac{dy}{dx} = -\frac{4h}{\rho u c_p D_h} y$$

for which the solution is

$$y(x) = \exp\left(-\frac{4h}{\rho u c_p D_h} x\right)$$

The temperature difference is reduced to a fraction, e^{-1} = 0.3679, of its initial value over a length scale,

$$x_{exp} = \frac{\rho u c_p D_h}{4h}.$$

The temperature difference is reduced to only 5% of its initial value over three times this length scale

$$x_5 = \frac{3\rho u c_p D_h}{4h}.$$

The convective heat transfer length scale formula is first applied to the flow inside of the micro-leaks. Choking is assumed to occur at the micro-leak exit into the sodium channel. Behind the choke point, the pressure decreases from 20 MPa inside of the CO_2 channel to the pressure at the choke point. In the current estimate, the pressure is set equal to 20 MPa, assuming that most of the reduction in pressure associated with the exit occurs near the choke point at the exit. The initial CO_2 temperature is set equal to the low value for the heat exchanger. The mass flux through the channel is equal to that calculated for critical flow with the modeling in the ANL Plant Dynamics Code.

Table 5 shows the mass flux results calculated for flow through the two assumed micro-leak channels for the AFR-100. The Reynolds number is readily calculated from the mass flux, ρu, as Re= ρuDh/μ.

Since the flow is turbulent, the forced convection heat transfer coefficient is assumed to be given by the Gnielinski correlation (Gnielinski, 1975; Todreas and Kazimi, 1990),

$$Nu = \frac{h D_h}{k} = \frac{\frac{f}{2}(Re - 1000)\,Pr}{1 + 12.7\left(\frac{f}{2}\right)^{\frac{1}{2}}\left(Pr^{\frac{2}{3}} - 1\right)}\left[1 + \left(\frac{D_h}{L}\right)^{\frac{2}{3}}\right]\left(\frac{Pr}{Pr_{wall}}\right)^{0.11}$$

where Nu and h are the mean Nusselt number and forced convection heat transfer coefficient, respectively, over the channel length, L. The Prandtl number is $Pr=c_p\mu/k$.

The friction factor, f, is given by the Blasius friction factor $f=0.0791/Re^{0.25}$.

In the present assessment, the difference between the Prandtl numbers evaluated with bulk fluid properties and properties at the wall in the Nusselt number correlation is neglected.

Thus, the last term is replaced by unity. The next to last term accounts for channel entrance effects.

Table 5 shows the length scale results calculated for the two assumed micro-leaks for AFR-100 heat exchanger low temperature conditions. The Reynolds numbers indicate turbulent flow. The calculated exponential length scales are 1.78 and 1.35 mm for the 25 and 113 µm circular holes, respectively. The distance separating the CO_2 and sodium channel could be as small as 1 to a few mm. It is possible that the flowpath through a microcrack could be tortuous resulting in an effective channel length that is longer than the distance between the CO_2 and sodium channels. The calculated exponential length scales are thus comparable to the micro-leak channel lengths. Thus, if the CO_2 expands as it flows down the micro-leak channel, cooling the CO_2, heat transfer from the surrounding stainless steel can heat the CO_2.

The decrease in pressure as CO_2 flows down a micro-leak channel limited by critical flow at the exit can be estimated as

$$\Delta P = \frac{4\tau L}{D_h} = \frac{2\rho u^2 f L}{D_h}$$

where

ΔP = pressure drop,

$\tau = \frac{1}{2}\rho u^2 f$ = shear stress.

For the two micro-leaks, the calculated pressure drops over a 1 mm length are 4.67 and 6.25 MPa, respectively. The estimated pressure drops are significant fractions of the initial 20 MPa pressure such that significant expansion and heat transfer are indicated for flow through the micro-leak channels.

Table 5: Convective heat transfer length scales of S-CO_2 through micro-leak

Micro-leak	25 µm hole	113 µm hole
Hydraulic Diameter, µm	25	19.8
Pressure, MPa	20	20
Temperature, °C	373	373
Mass Flux, kg/(m^2·s)	40,100	40,100
Density, kg/m^3	164	164
Specific Heat, J/(kg·K)	1,230	1,230
Viscosity, Pa·s	3.23×10^{-5}	3.23×10^{-5}
Thermal Conductivity, W/(m·K)	0.0513	0.0513
Prandtl Number	0.773	0.773
Velocity, m/s	244	244
Reynolds Number	31,030	24,600
Blasius Friction Factor	0.00596	0.00632
Channel Length, m	0.001	0.001
Hydraulic Diameter-to-Channel Length Ratio	0.025	0.0198
Hydraulic Diameter-to-Channel Length Ratio Factor	1.0855	1.0732
Nusselt Number	84.3	69.6
Heat Transfer Coefficient, W/(m^2·K)	1.73×10^5	1.80×10^5
Exponential Length Scale, m	0.00178	0.00135
5 % Length Scale, m	0.00534	0.00405

3.2.3 Heat transfer in voided sodium channel

Length scales for forced convection heat transfer were also calculated for CO_2 flowing through a voided sodium channel. The pressure inside of the channel is assumed to be one atmosphere and the CO_2 properties are evaluated at the mean temperature of the isentropic expansion. As discussed above, this is expected to be lower than the actual mean temperature due to the reduction in CO_2 pressure due to wall friction and heat transfer from stainless steel to CO_2 as it flows through the micro-leak channel. The CO_2 is assumed to flow both up and down the voided sodium channel away from the micro-leak location. The CO_2 mass flux in each direction through the voided sodium channel is thus

$$\rho u = G_{channel} = \frac{G_{leak} A_{leak}}{2 A_{channel}}$$

where

G denotes mass flux and A_{leak} and $A_{channel}$ are the flow areas through the micro-leak and sodium channel.

For the 25 µm circular hole, the CO_2 velocity through the sodium channel is so low that the flow is laminar. The Nusselt number is assumed to be given the correlation of Lee and

Garimella for a rectangular channel (Lee and Garimella, 2006). The Nusselt number for fully developed laminar flow is

$$\mathrm{Nu}_{\infty} = 8.235\left(1 - \frac{2.0421}{e} + \frac{3.0853}{e^2} - \frac{2.4765}{e^3} + \frac{1.0578}{e^4} - \frac{0.1861}{e^5}\right)$$

where

$$e = \frac{\text{channel height}}{\text{channel width}} > 1.$$

Greater Nusselt numbers exist in the thermal entrance region having a length defined as that where the Nusselt number drops to a value 5 % above the fully developed value. Defining a non-dimensional distance as

$$x^* = \frac{x}{\mathrm{Re} D_h \mathrm{Pr}}$$

the thermal entrance length is given by

$$x^*_{th} = -1.275\times10^{-6}e^6 + 4.709\times10^{-5}e^5 - 6.902\times10^{-4}e^4 + 5.014\times10^{-3}e^3 - 1.769\times10^{-2}e^2 + 1.845\times10^{-2}e + 5.691\times10^{-2}$$

Results for AFR-100 and AFR-1000 conditions are shown in Table 6. The Reynolds numbers are only about 100 indicating laminar flow. The thermal entrance lengths are only about 2 cm. Using the heat transfer coefficients for fully developed flow, the exponential length scales for forced convection heat transfer are only about 2 cm and the 5 % length scales are only about 7 cm. Given the small 5 % length scales, it is expected that the CO_2 cooled by expansion would be effectively heated by the surrounding heat sinks as it flows down the channel.

Table 6: Convective heat transfer length scales for S-CO_2 exiting 25 µm hole through sodium channel

Reactor Plant	AFR-100	AFR-1000
Hydraulic Diameter, mm	4.8	4.8
Channel Aspect Ratio	1.5	1.5
Pressure, MPa	0.101325	0.101325
Temperature, °C	152	127
Mass Flux, kg/(m^2·s)	0.410	0.410
Density, kg/m^3	1.26	1.34
Specific Heat, J/(kg·K)	962	942
Viscosity, Pa·s	2.08×10^{-5}	1.97×10^{-5}
Thermal Conductivity, W/(m·K)	0.0273	0.0251
Prandtl Number	0.734	0.738
Velocity, m/s	0.325	0.306
Reynolds Number	94.6	100
Nusselt Number Aspect Ratio Factor	0.461	0.461
Nusselt Number for Fully Developed Flow	3.79	3.79
Heat Transfer Coefficient, W/(m^2·K)	21.6	19.9
Dimensionless Entrance Length	0.0586	0.0586
Entrance Length, m	0.0196	0.0207
Exponential Length Scale, m	0.0220	0.0233
5 % Length Scale, m	0.0659	0.0700

3.2.4 Isenthalpic expansion

The potential for significant heat transfer from stainless steel to CO_2 as it flows through the micro-leaks implies that final CO_2 temperatures calculated assuming an isentropic expansion are expected to be overly conservative; that is, they are overly conservative lower bounds to the final CO_2 temperatures. As an alternative to isentropic flow, critical flowrates and conditions following expansion are sometimes calculated assuming isenthalpic flow. Temperatures and reductions in temperature for an isenthalpic expansion are shown in Table 7. The calculated temperature reductions are remarkably low compared with those for isentropic expansion in Table 4. Furthermore, the calculated reductions in temperature are virtually the same for isenthalpic expansions down to atmospheric pressure, 0.1 MPa.

The fact that the exponential length scales for forced convection heat transfer are greater than one mm indicates that heat transfer, while significant, would not be complete in heating the CO_2 back up to the stainless steel temperature. It follows that the flow would not be isothermal. Since isenthalpic flow also implies effective heat transfer, an isenthalpic expansion assumption is also expected to be conservative in requiring too much heat exchange. The reality of critical flow and expansion is therefore expected to be somewhere

between the extremes of isentropic and isenthalpic flow. However, since constant properties are assumed in both the isentropic and isenthalpic analyses, there are certain situations where they don't necessarily represent the bounding cases. This holds true for the pressure drop calculations above as well since there will be significant differences in the density of the CO_2 between 20 MPa and 0.1 MPa. As mentioned previously, a meshed-iterative scheme that includes conjugate heat transfer would be the next step in more accurately modeling this process.

Table 7: Final states and temperatures of CO_2 following isenthalpic expansion through micro-leak

Reactor	AFR-100	AFR-100	AFR-1000	AFR-1000
Initial CO_2 Pressure, MPa	20	20	20	20
Initial CO_2 Temperature, °C	528	373	484	332
Initial CO_2 Specific Enthalpy, kJ/(kg·K)	1007.7	816.95	953.35	766.74
Final CO_2 State Following Expansion to 0.1 MPa	Gas	Gas	Gas	Gas
Final CO_2 Temperature Following Expansion to 0.1 MPa, °C	512	343	465	296
Temperature Reduction Following Expansion to 0.1 MPa, °C	16	30	19	36

3.2.5 Voiding of the affected sodium channel

The results presented immediately above show that CO_2 released from a micro-leak and flowing through a voided sodium channel will be significantly heated while flowing through the sodium channel. The stainless steel, sodium, and CO_2 in the intact portion of the heat exchanger surrounding the sodium channel containing the micro-leak will act as a massive heat sink that serves to heat up the released CO_2. To obtain the estimates below, it is presently assumed that the CO_2 is heated all the way to the surrounding heat exchanger temperature.

The density of the expanded CO_2 can be estimated from the ideal gas equation,

$$\rho = \frac{P_{Na}}{R_{gas} T_{Na}},$$

where

P_{Na} = intermediate sodium system pressure,

R_{gas} = gas constant for CO_2,

T_{Na} = intermediate sodium system temperature.

The specific volume of the expanded CO_2 is the inverse of the density,

$$v = \frac{1}{\rho}.$$

The expanded CO_2 volume addition rate into the sodium channel containing the micro-leak is

$$\frac{dV}{dt} = v\, G_{leak}\, A_{leak},$$

where:

G_{leak} = mass flux through the micro-leak,

A_{leak} = effective flow area of micro-leak.

The CO_2 mass flux through the leak is taken equal to that at the low temperature of the heat exchanger as in the analyses above. Table 8 and
Table 9 show the resulting expanded CO_2 volume addition rates for this same break mass flux at the high and low heat exchanger temperatures and at an assumed intermediate sodium loop pressure of 0.5 MPa for AFR-100 and AFR-1000 conditions, respectively.

The AFR-100 has a high sodium temperature above 500 °C for which reaction between sodium and CO_2 might not produce any gaseous reaction products. That case shall be discussed separately. First, the case where the reactions occur as expected at lower temperatures shall be assessed. Thus, for the AFR-100 case, it is first assumed that the threshold temperature at which the nature of the sodium-CO_2 interactions changes is above the high temperature.

For the 25 µm circular hole, the CO_2 volume addition rates to the channel are comparable to the sodium volume flowrate through the channel. For the 113 µm hole, the CO_2 volume addition rates are significantly greater than the sodium volume flowrate through the channel. Immediately following the assumed sudden formation of the micro-leak, the expansion of CO_2 inside of a single sodium channel is expected to fill the volume of the channel in the vicinity of the micro-leak. The accumulating CO_2 is expected to void the currently assumed vertical channel both in the downward and upward directions. Although there is a pump driving head behind the intermediate sodium loop flow upstream of the intermediate heat exchanger, each sodium-to-CO_2 heat exchanger unit contains many parallel sodium channels (5330 channels estimated for the AFR-1000). Thus, each compact diffusion-bonded heat exchanger is a massively parallel flow channel system. The expansion of the CO_2 void inside of a single sodium channel will readily result in diversion of the sodium flow from the failed sodium channel into other sodium channels. Thus, the CO_2 will void the channel containing the micro-leak in both the downward and upward directions.

The growing CO_2 void region in the sodium channel containing the micro-leak is approximated by slug bubble fronts moving upward and downward in the failed channel. The front velocity of the slug bubbles can be estimated as the CO_2 volume addition rate divided by twice the flow area of a single sodium channel,

$$v_{front} = \frac{\frac{dV}{dt}}{2 A_{channel}} .$$

This estimate of the front velocity is an underestimate. In reality, the entire cross-sectional area of the sodium channel will not be occupied by void. As the slug bubble fronts move up and down the channel, a sodium film will be left upon the channel walls behind each of the fronts. For bubbles driven by buoyancy and rising inside of water draining from vertical circular tubes, Davies and Taylor (1950) found that a water film was left behind on the inner cylindrical wall. The films slowly drained with time. The initial film thickness behind the rising slug bubble front was measured to be as large as 17.1 % of the tube inner radius. For the 4 mm by 6 mm H2X sodium channel, the hydraulic diameter is 4.83 mm. A fraction, 0.171, of half of this diameter gives a roughly estimated sodium film thickness of 0.41 mm behind each slug bubble front.

Table 8: Release of CO_2 into sodium channel of IHX of AFR-100 through microleaks

Micro-leak	**25 µm hole**	**113 µm hole**
Intermediate Sodium Pressure, MPa	0.5	0.5
Intermediate Loop High Temperature, °C	528	528
Intermediate Loop Low Temperature, °C	373	373
CO_2 Volume Addition Rate at High Temperature, m^3/s	5.96×10^{-6}	1.21×10^{-4}
CO_2 Volume Addition Rate at Low Temperature, m^3/s	4.81×10^{-6}	9.79×10^{-5}
Slug Bubble Front Velocity at High Temperature, m/s	0.124	2.53
Slug Bubble Front Velocity at Low Temperature, m/s	0.100	2.04
Homogeneous Flow Void Fraction for Nominal Single Channel Sodium Flow at High Temperature	0.689	0.978
Homogeneous Flow Void Fraction for Nominal Single Channel Sodium Flow at Low Temperature	0.650	0.974
Homogeneous Flow Void Fraction for Nominal Heat Exchanger Sodium Flow at High Temperature	4.16×10^{-4}	8.40×10^{-3}
Homogeneous Flow Void Fraction for Nominal Heat Exchanger Sodium Flow at Low Temperature	3.48×10^{-4}	7.03×10^{-3}

As shown in Table 8 and
Table 9, the bubble front velocities for the 25 µm diameter hole results in front velocities of 0.117 and 0.0938 m/s for CO_2 at the high and low sodium temperatures of the AFR-1000, respectively. This may be compared with the 0.112 and 0.108 m/s nominal sodium velocities

downward through an intact channel at the hot and cold ends, respectively. For the 113 µm hole, the CO_2 front velocities are 2.39 and 1.91 m/s at the high and low temperatures of the AFR-1000, respectively.

The sodium left behind as a film will be subjected to the gravitational force and will slowly drain downward. However, the sodium film will also chemically react with the CO_2 flowing over it. In the impingement zone of CO_2 discharging from the micro-leak, the low CO_2 temperature resulting from expansion may tend to reduce the rate of chemical reactions. However, away from the impingement zone, heating of the CO_2 will tend to raise the flowing CO_2 temperature back toward the surrounding structure temperatures. The production of solid reaction products including sodium carbonate, sodium oxide, and carbon may result in the formation of a solid layer on the walls of the failed sodium channel as well as the formation of some CO that enters the flowing gas streams.

Table 9: Release of CO_2 into sodium channel of IHX of AFR-1000 through microleaks

Micro-leak	**25 µm hole**	**113 µm hole**
Intermediate Sodium Pressure, MPa	0.5	0.5
Intermediate Loop High Temperature, °C	484	484
Intermediate Loop Low Temperature, °C	332	332
CO_2 Volume Addition Rate at High Temperature, m^3/s	5.63×10^{-6}	1.15×10^{-4}
CO_2 Volume Addition Rate at Low Temperature, m^3/s	4.50×10^{-6}	9.17×10^{-5}
Slug Bubble Front Velocity at High Temperature, m/s	0.117	2.39
Slug Bubble Front Velocity at Low Temperature, m/s	0.0938	1.91
Homogeneous Flow Void Fraction for Nominal Single Channel Sodium Flow at High Temperature	0.677	0.977
Homogeneous Flow Void Fraction for Nominal Single Channel Sodium Flow at Low Temperature	0.635	0.973
Homogeneous Flow Void Fraction for Nominal Heat Exchanger Sodium Flow at High Temperature	3.93×10^{-4}	7.94×10^{-3}
Homogeneous Flow Void Fraction for Nominal Heat Exchanger Sodium Flow at Low Temperature	3.26×10^{-4}	6.59×10^{-3}

Voiding of the channel near the micro-leak removes the presence of sodium filling the bulk channel immediately in front of the micro-leak. Although sodium is left behind as a sodium film on the wall on the sides of the micro-leak, the mass of remaining sodium is limited. This is expected to reduce the potential for self-plugging of the micro-leak to occur due to the formation of solid reaction products (e.g., carbonate). If self-plugging occurs, it needs to take place due to the formation of solid reaction products in the film layer remaining at the wall at the micro-leak location. It is difficult to see how the structural strength of such a layer could resist the pressure drop between the pressure at the choke point and the low pressure inside of the voided sodium channel.

Table 8 and
Table 9 also include the CO_2 volume fraction when the released CO_2 is assumed intermixed with all of the sodium flowing through one heat exchanger unit. The CO_2 void fraction is calculated from the CO_2 volume addition rate and nominal sodium volume flowrate through one heat exchanger unit assuming that the CO_2 and sodium flow with the same velocity (zero slip).

If the sodium temperature is above the threshold for a change in the nature of the chemical reactions at about 500 °C, then the reaction of CO_2 and sodium can ultimately produce only solid reaction products of sodium oxide and elemental carbon; that is, there are no gaseous reaction products. However, this requires that the sodium and CO_2 can continue to interact at this temperature for a sufficiently long time for the reactions to go to completion. If the reaction is slow enough, CO_2 will still collect in front of the micro-leak and initiate voiding of the channel. The low temperature of CO_2 discharging from the micro-leak might also contribute to reducing the reaction rate in the immediate vicinity of the micro-leak. In this case, the reaction will be limited to the slug bubble fronts advancing through the sodium channel and the sodium films left behind on the sodium channel walls. For CO_2 flowing upward through the sodium channel, gaseous CO_2 above the reaction threshold temperature might still discharge into the inlet sodium header. Interaction with hot sodium inside of the inlet sodium header may result in complete reaction of the CO_2 with hot sodium. One can envision a void region inside of the inlet sodium header with bubble formation such that CO_2 reacts with sodium to form the solid reaction products and no gaseous reaction products.

The CO_2 flowing downward through the sodium channel will be cooled to temperatures below the approximately 500 °C reaction threshold changing the nature of the chemical reactions to those forming CO as a gaseous reaction product.

It might be that the chemical reactions above the reaction threshold temperature are essentially instantaneous. In such a case, the CO_2 discharging from the micro-leak might be consumed through reaction near the micro-leak. Experiments in the SNAKE facility are needed to determine the extent of CO_2 penetration into hot sodium at a temperature above the reaction threshold temperature before the CO_2 is consumed.

The upward and downward flowing mainly CO_2 gas streams will exit the sodium channel containing the micro-leak at both the top and bottom of the heat exchanger core and enter the header plenum sodium volumes above and below the core. The gas entering the header plenum will spread as it penetrates downward into the header due to intermixing with sodium forming CO_2 bubbles.

3.2.6 Bubble behavior in sodium

A bubble of CO_2 that forms from interactions of the CO_2 jet with sodium can be entrained into the sodium, if the local sodium velocity exceeds the rise velocity of the bubble due to

buoyancy. Rodrigue (2001) derived a correlation for the bubble terminal rise velocity in an infinite fluid medium. His correlation is based upon 897 data points covering the ranges,

$722 < \rho_c < 1{,}380$ kg/m^3,
$2.2 \times 10^{-4} < \mu c < 18$ Pa·s,
$0.0159 < \sigma < 0.091$ N/m,
$1.9 \times 10^{-7} < Re < 1.1 \times 10^4$,
$1.0 \times 10^{-11} < M < 1.0 \times 10^7$.

The bubble Reynolds number and Morton number are defined by

$$Re = \frac{\rho_c U_t d}{\mu_c}$$

and

$$M = \frac{g \Delta\rho \mu_c^{\,4}}{\rho_c^{\,2} \sigma^3}$$

where

ρ_c = density of continuous fluid,
U_t = bubble terminal rise velocity,
d = bubble diameter,
μc = viscosity of continuous fluid,
g = gravitational acceleration,

$\Delta\rho = \rho_c - \rho$,

σ = surface tension at interface.

Other non-dimensional groups for bubbles are the Eötvös number,

$$Eo = \frac{\rho_c g d^2}{\sigma},$$

and the capillary number,

$$Ca = \frac{\mu_c U_t}{\sigma}.$$

Rodrigue's correlation is

$$V = \frac{\frac{1}{12} F}{1 + 4.9 \times 10^{-2} F^{\frac{3}{4}}}$$

where the velocity number, V

$$V = U_t \left(\frac{\rho_c{}^2 d^2}{\mu_c \sigma} \right)^{\frac{1}{3}},$$

and the flow number

$$F = g \left(\frac{\rho_c{}^5 d^8}{\mu_c^4 \sigma} \right)^{\frac{1}{3}},$$

are two new non dimensional numbers that Rodrigue obtained.

Terminal rise velocities were calculated for bubbles inside of sodium at the low temperature for the intermediate circuit of the AFR-1000. The Morton number does not depend upon the bubble diameter or terminal rise velocity and is equal to 2.09×10^{-14}. Figure 3 shows the dependency of the bubble terminal rise velocity upon the bubble diameter. The table also shows the values and dependencies of the other non-dimensional groups. As expected, small bubbles with diameters of 0.1 mm or less have small terminal rise velocities. As discussed by Rodrigue (2001) for $F << 1$, the flow is laminar and the terminal rise velocity varies as the square of the bubble diameter. When $F >> 1$, the flow is turbulent and the terminal rise velocity is independent of the bubble diameter. As seen from Figure 3, the terminal rise velocity effectively attains a maximum value independent of the bubble diameter for bubble diameters of about 2 mm and greater. The maximum bubble terminal rise velocity is 0.359 m/s. Thus, a downward sodium velocity greater than 0.36 m/s would be expected to sweep bubbles of any size downward preventing their rise upward through the flowing sodium.

The terminal rise velocity of a bubble inside of a channel is less than that inside of an infinite medium. In deriving his correlation, Rodrigue applied a correction to data assuming that the ratio of the terminal velocity inside of a container to the terminal velocity in an infinite medium is given by

$$\frac{U_{t,container}}{U_t} = \left(1 - \left(\frac{d}{D_{container}} \right)^2 \right)^{\frac{3}{2}}$$

where $D_{container}$ is the container diameter while excluding data for which the diameter ratio exceeded 0.1.

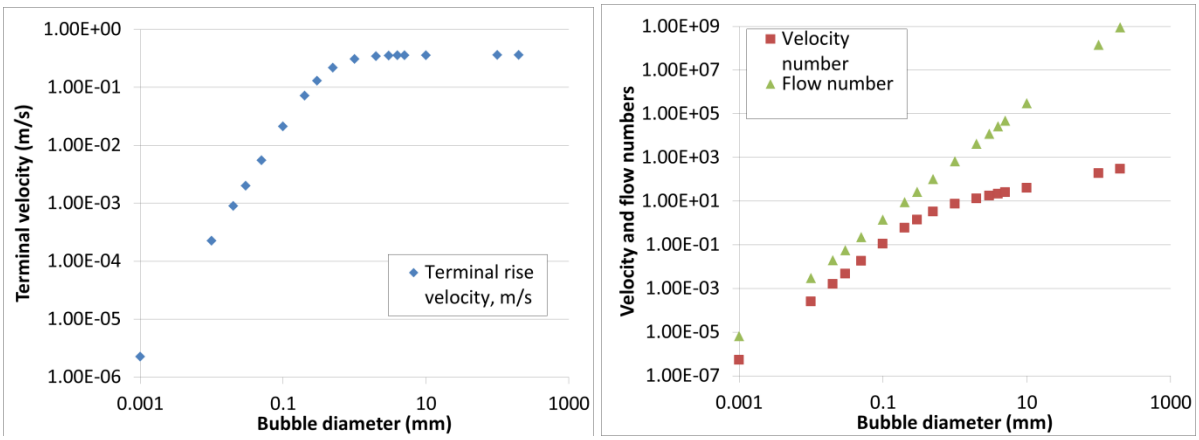

Figure 3: Terminal rise velocity (left) and velocity and flow numbers (right) for CO_2 bubbling inside the IHTS of AFR-1000

3.2.7 Carbon dioxide behavior inside heat exchanger headers

The CO_2 flowing upward from the affected sodium channel enters the overlying sodium inlet header. The upward flowing CO_2 will form a jet that expands with height as CO_2 intermixes with generally downward flowing sodium forming CO_2 bubbles. The rise velocity of the largest sodium bubbles is 0.36 m/s or less which is significantly less than the 2.9 m/s velocity of the sodium entering the header through the sodium inlet pipe. Thus, the bubbles cannot rise upward into the incoming sodium flow inside of the pipe or near the top of the header.

It is expected that the size of the CO_2 gas region inside of the inlet header will grow to a maximum size. At this maximum size, the sodium will be largely diverted around the gas region. This process may result in starvation of the flow of sodium to a number of sodium channels near the affected channel. Reduction of the number of channels with sodium flow will generally increase the sodium velocity through the remaining channels. Sufficiently small sodium bubbles formed may be entrained into the downward sodium flow and carried downward through sodium channels in the heat exchanger core. For example, this would be the case for bubbles having diameters less than 0.05 mm.

The CO_2 flowing downward from the affected sodium channel enters the underlying sodium outlet header. The CO_2 expands as a jet as it intermixes with surrounding sodium forming CO_2 bubbles. As discussed above, immediately below the heat exchanger core, the one-dimensional sodium velocity downward is only 0.0441 m/s. Bubbles having diameters greater than about 0.2 mm formed in this location will rise upward through the downward flowing sodium. Bubbles with diameters greater than about 0.3 mm have terminal rise velocities greater than the 0.108 m/s nominal sodium velocity inside of the sodium channels. Thus, bubbles immediately beneath the heat exchanger core can rise up into adjacent sodium channels and even rise completely through the channels into the overlying sodium inlet header.

Inside of the sodium outlet header, the surface area of the mainly downward CO_2 jet increases with penetration downward. The sodium downward velocity increases with distance

downward due to the smaller cross-sectional flow area inside of the header tending toward the 2.9 m/s sodium velocity in the circular outlet pipe beneath the header. It is expected that an equilibrium will develop in which the size of the CO_2 gas regions inside of the inlet and outlet headers grow to maximum sizes at which the overall rate of entrainment of CO_2 by sodium to be carried into the outlet pipe equals the rate of addition of CO_2 through the micro-leak. As observed from Table 8 and Table 9, the CO_2 volume fraction for incorporation of the CO_2 release rate into the nominal sodium volume flowrate for a heat exchanger unit is rather small being less than 0.01 for the assumed 113 µm hole. For the 25 µm circular hole, the CO_2 volume fraction is even smaller being less than 0.0005.

It is possible that the entrainment rate of CO_2 bubbles might not reach the rate of CO_2 addition. In such a case, the CO_2 volume inside of the headers grows and pressurizes the heat exchanger unit to a sufficient level to divert the incoming sodium flow to other heat exchanger units. This is possible because the heat exchanger units form a massively parallel flow channel system. In such a case, the CO_2 volume will grow inside of the headers and ultimately displace sodium through the sodium outlet pipe.

3.2.8 Chemical reactions

The released CO_2 will have little sodium to react with inside of the affected sodium channel. Reaction will be limited to the front of the CO_2 slug bubbles and with sodium left behind as a film upon the channel walls, with the possible exception of CO_2 released at an elevation where the sodium temperature is above the reaction threshold temperature of about 500 °C. The main chemical reactions occur inside of the sodium headers as the CO_2 intermixes with sodium, and inside the remainder of the intermediate sodium loop as CO_2 bubbles are entrained and transported in the flowing sodium.

A fundamental question concerns the rates at which CO_2 reacts with sodium for CO_2 jets and bubbles of different sizes. Experiments in which CO_2 is injected into sodium in the SNAKE sodium-CO_2 interaction facility will be necessary to answer this question. For the present, it is assumed that the reactions are not instantaneous such that they continue as CO_2 bubbles and are transported through the intermediate sodium loop. The effective rates will depend upon the effective surface-to-volume ratio for the distribution of bubble sizes transported through the sodium.

For the case where the sodium temperatures inside the intermediate sodium loop are all below the 500 °C reaction threshold temperature, complete reaction of the CO_2 produces ½ mole of CO for each mole of CO_2. Complete reaction to CO would thus decrease the volume fraction of gas in the flowing sodium by 50 %. It is speculated here that continued transport of CO in the sodium might enable the CO to react with the sodium to form sodium oxide and elemental carbon. If so, then the gas could eventually be consumed through chemical reactions.

Reactions might not go to completion or their rates could be reduced, if there are mechanisms for CO_2 or CO bubbles to be separated from the sodium flow such that the gas can collect in regions having relatively little interfacial exposure to sodium. For example, this could happen

at the sodium surface of a sodium expansion vessel. Gas bubbles entrained in the sodium flow will be transported through sodium channels of heat exchanger units. Because the sodium velocity is low inside of the headers adjacent to the core, gas could collect as large bubbles inside of sodium inlet headers.

Chemical reaction rates generally increase with increasing temperature. Exceptions are situations in which the reaction rates are limited by mass transport such as diffusion or convection of a gas species within a bubble. In general, greater rates of reaction are expected as the CO_2 and CO flow through the higher temperature portions of the intermediate sodium loop including the hotter parts of the intermediate heat exchanger (IHX), piping connecting the IHX to the sodium-to-CO_2 heat exchanger units, and the hotter parts of the heat exchanger units.

Above 500 °C, chemical reaction of CO_2 with sodium consumes all of the gas. However, the CO_2 is not maintained in contact with sodium at temperatures above the 500 °C threshold temperature. The entrained CO_2 is transported around the intermediate sodium loop at the intermediate loop temperatures spending only a portion of the transit time above 500 °C. Thus, while the temperature is below the 500 °C threshold temperature, a portion of the CO_2 can be converted to CO. When the CO_2 is transported into the portion of the loop above 500 °C, it is possible for part of the CO_2 to be completed reacted to form only solid reaction products.

4 Formulation of general test matrix

A condensed overview of the proposed test matrix for the SNAKE facility is shown in Table 10. The total number of experiments (including water tests) proposed is 107, with 71 of them being sodium tests. This is a very ambitious proposal especially considering that each sodium test could take approximately 2-3 weeks including preparations, nozzle change-out, and cleaning. The exact test specifications will be decided and modified throughout the program in order to optimize and prioritize data.

Table 10: SNAKE test matrix (H=high/large, M=medium, L=low/small)

Water tests			
CO_2 stagnation pressure, MPa	CO_2 stagnation temperature, ˚C	Water temperature, ˚C	Configuration
H	H, L	H, L	Direct nozzle injection
M	H, L	H, L	Direct nozzle injection
L	H, L	H, L	Direct nozzle injection
H, L	H, L	H	Injection into sodium channel

CO_2 impingement on plate in air	
CO_2 stagnation pressure, MPa	CO_2 stagnation temperature & intial structure temperature, ˚C
H	H, M, L
L	H, M, L

CO_2 injection from micro-nozzle into open sodium pool			
CO_2 stagnation pressure, MPa	CO_2 stagnation temperature, ˚C	Sodium column temperature, ˚C	Sodium column height, m
H	H, M, L	H, L	H, L
M	H, M, L	H, L	H, L
L	H, M, L	H, L	H, L

CO/CO_2 mixture injection from micro-nozzle into open sodium pool			
Mixture	Nozzle size, µm	Sodium column temperature, ˚C	Sodium column height, m
0.5 CO_2 + 0.5 CO	H, L	H, L	H, L
CO	H, L	H, L	H, L

CO_2 injection from micro-nozzle into a sodium channel			
CO_2 stagnation pressure, MPa	CO_2 stagnation temperature, ˚C	Sodium column temperature, ˚C	Sodium column height, m
H	H	H	M
H	L	L	M
L	H	H	M
L	L	L	M

Long term reaction product behavior in flowing sodium		
Injected gas or solid	Nozzle size, µm	Sodium temperature, ˚C
CO_2	H, L	H, M, L
CO	H, L	H, M, L
Na_2CO_3	n/a	H, M, L

4.1 Water visualization & checkout tests

Visualization tests in which CO_2 is injected into a cylindrical water pool are planned to attempt to simulate the flow regime of CO_2 injected into sodium. To investigate one of the

differences resulting from the property differences between water and sodium, bubble rise velocities were calculated for water to compare with those for sodium in Figure 3. Relevant thermophysical properties for water (NIST, 2013) at one atmosphere and 25 °C (i.e., room temperature) and 95 °C (i.e., heated water with low subcooling) are compared with those for sodium (Fink and Leibowitz, 1995) in Table 11. At the lower temperature, the water viscosity is significantly greater than that of sodium. The water viscosity is close to that of sodium at the higher water temperature. The water surface tension is significantly lower than that of the liquid metal. However, the water surface tension decreases with increasing temperature such that a higher water surface tension is realized at the lower water temperature.

Table 11: Comparison of thermophysical properties of sodium and water

Fluid	Sodium	Water at 25 °C	Water at 95 °C
Temperature, °C	332	25	95
Density, kg/m^3	873	997	962
Viscosity, Pa·s	3.17×10^{-4}	8.90×10^{-4}	2.97×10^{-4}
Surface Tension, N/m	0.176	0.0720	0.0599

The case of water at one atmosphere and 25 °C (i.e., room temperature) is considered first. The bubble Morton number is 1.66×10^{-11}. Results are shown in Figure 4. It is observed that for the same bubble diameters, the bubble rise velocities in water at 25 °C are all lower than those in sodium. For example, for large bubbles, the rise velocity tends to 0.277 m/s versus 0.359 m/s in sodium. For a small bubble of 0.1 mm diameter, the rise velocity in 25 °C water is 8.86×10^{-3} m/s versus 2.12×10^{-2} m/s in sodium; that is, the rise velocity in water is less than half that in sodium. The bubble Reynolds numbers for bubbles in water are significantly lower than the bubble Reynolds numbers at the same bubble diameters in sodium.

The bubble rise velocities in water can be increased by increasing the subcooled water temperature. Figure 4 shows the rise velocities calculated for water at one atmosphere pressure and 95 °C temperature. The bubble Morton number is 3.71×10^{-13}. The calculated bubble rise velocities in water at 95 °C are closer to those calculated for sodium. For bubble diameters of 0.2 mm and smaller, the rise velocity in water is actually greater than that in sodium. At 0.1 mm, the rise velocity in water is 0.0241 m/s versus 0.0212 in sodium. For bubble diameters of 0.3 mm and larger, the rise velocity in water is less than that in sodium. In the limit of large bubbles of 2 mm diameter or greater, the rise velocity in water tends to 0.267 m/s versus 0.359 in sodium. Interestingly, at 25 °C, the rise velocity tends to a greater value of 0.277 m/s for large bubbles. At 95 °C, the bubble Reynolds numbers in water are close to the bubble Reynolds numbers in sodium. This reflects the similar values of the viscosities of water at 95 °C and sodium.

The results indicate that for the bubble rise velocity, water provides a better simulation of sodium when the water is heated such that the water viscosity is similar to the sodium viscosity. In the present case, heating the water to 95 °C such that there is a small subcooling of 5 °C provides a suitably close matching of viscosities.

The simulation is not perfect because the water surface tension is significantly lower than that of sodium (0.0599 N/m at 95 °C for water versus 0.176 N/m for sodium). This suggests

investigating the effects of adding surfactants to the water to increase the surface tension. If the surface tension can be increased to a value similar to that for sodium, then the heated water might provide a better simulation of the bubble behavior and flow regime for sodium.

The proposed water test matrix in Table 10 includes a combination of high and low CO_2 pressures & water temperatures at three different CO_2 stagnation pressures. Video recording of the bubble behavior would be necessary in order to document the bubble size, velocity, and behavior in water.

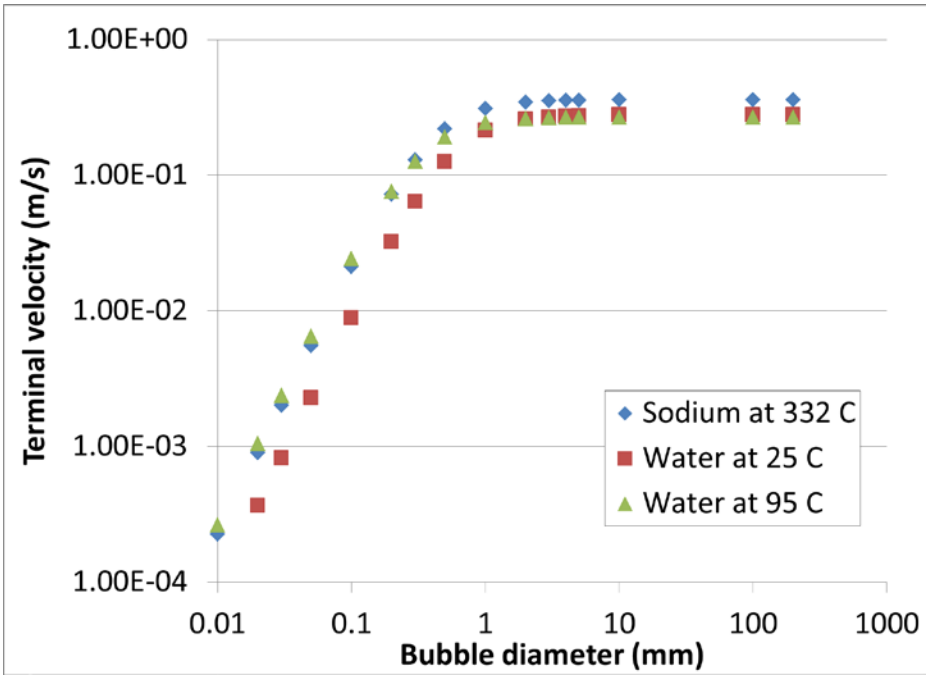

Figure 4: Terminal rise velocity comparison between sodium and water

4.2 CO_2 impingement/thermal shock tests

The above analysis has shown that the CO_2 temperature may decrease significantly as the CO_2 expands while flowing through a micro-leak channel and subsequently after exiting the micro-leak channel. However, the maximum temperature reductions calculated assuming an isentropic expansion may be mitigated by heat transfer from surrounding structure to the flowing CO_2. Experiments are needed to measure the CO_2 temperature impinging upon stainless steel structure opposite a micro-leak. The experiments would be performed without sodium in air.

Initial tests can employ a stainless steel target plate opposite the micro-leak nozzle. The plate should be heated to the same temperature as the stagnation temperature of the CO_2 using a large copper block with embedded heaters. A thermocouple can be mounted with an exposed junction at the CO_2 impingement point to measure the temperature of the impinging expanded CO_2. Other thermocouples can measure the CO_2 temperature at increasing radial distances from the impingement point. The initial CO_2 and stainless steel temperatures should be varied

over high, medium, and low values representative of a sodium-to-CO_2 heat exchanger. For example, the high and low values may be chosen as the bounding values of 510 and 332 °C, respectively. The medium value may be set equal to an intermediate temperature.

The nozzle itself should be surrounded by a large copper block with controlled temperature in order to mimic the expected boundary conditions in the heat exchanger. Since the tests will be completed in room temperature air, the large copper blocks around the nozzle and impinged plate make temperature control possible. The small distance between the nozzle and plate, up to 6 mm to represent the sodium channel distance, will also make temperature control possible.

For all tests, temperature data may be compared with first principles predictions based upon isentropic, isenthalpic, and isothermal flow through the micro-leak channel. More detailed thermal hydraulic analyses could also be performed for the flow through the micro-leak channel to calculate the heat transfer from the surrounding stainless steel to the flowing CO_2 bypassing the need for idealized assumptions of isentropic, isenthalpic, or isothermal flow.

A test matrix for the CO_2 impingement/thermal shock tests is provided in Table 10. Temperatures are currently specified as High, Medium, and Low because actual temperatures achievable in SNAKE may be subject to operating considerations or constraints such as the maximum design temperature. High and low pressure CO_2 injection should be carried out at each temperature.

4.3 CO_2 injection from micro-nozzle into open sodium pool

Experiments with direct injection of CO_2 from nozzles into the sodium column are identified mainly to investigate the interaction and kinetics of CO_2 with sodium at different temperatures. These tests would focus on testing a range of CO_2 pressures and temperatures injected from various nozzle sizes into a range of sodium column heights. These tests will make it possible to gain an understanding of the reaction thresholds and kinetics. They can also be used to study gas hold-up in the column.

Table 10 shows a test matrix for direct injection of CO_2 into sodium. It is realized that as written the test matrix implies a large number of thirty six experiments. It is hoped that this number can be significantly reduced based upon the experience with the first few experiments. For example, it might be found that for the small nozzle sizes, the injected bubbles are small and reactions occur rapidly or that the bubble rise velocity is so small that complete reaction takes place within a small sodium height. This would eliminate the need for varying the sodium column height thereby reducing the number of tests. More tests may be added to precisely determine a threshold temperature for a change in the nature of chemical reactions such as around 450-500 °C.

4.4 CO/CO_2 mixtures injection from micro-nozzle into open sodium pool

Experiments with direct injection of CO/CO_2 mixtures from nozzles into the sodium column are identified in order to investigate the interaction and kinetics of CO with sodium at different temperatures. The gas composition is varied in order to simulate partial reaction of the CO_2 with sodium and study the mixture reaction with sodium. This effectively simulates increased reaction time without necessitating a taller sodium column.

Table 10 shows a test matrix for direct injection of CO/CO_2 mixtures into sodium. As written the test matrix includes 16 experiments. It is hoped that this number can be significantly reduced based upon the experience with the first few experiments. This number could be slightly reduced or increased to study additional gas compositions once the initial data is examined.

4.5 CO_2 injection from micro-nozzle into a sodium channel

Experiments are needed that simulate release of CO_2 from a micro-leak into a single vertical compact diffusion bonded heat exchanger sodium channel followed by flow of the CO_2 into either the sodium inlet header above the heat exchanger core or the sodium outlet header below the heat exchanger core. Since the CO_2 injection line is currently installed near the bottom of the sodium interaction vessel, initial tests should inject CO_2 into a vertical single stainless steel sodium channel near the bottom of the interaction vessel. The sodium channel should be closed off at the bottom such that CO_2 and sodium flow upward into the sodium pool provided by the sodium column in the overlying part of the interaction vessel. The sodium channel could extend up to approximately 10 cm above the CO_2 injection point recognizing that in a heat exchanger having a Z configuration there exists a region of similar height over which the CO_2 flow transitions from generally sideward to vertical.

The exact maximum height of the channel is dependent on the ports available on the test vessel. The maximum channel height that can easily be installed by simply slipping the nozzle and channel assembly in through the 2 inch diameter port at the bottom of the test vessel is just over 2.54 cm. Any channel that is longer than this would require additional manipulation and installation of the channel onto the nozzle internally to the test vessel. While possible, this could be a very difficult procedure. If solid reaction products build up during the test, it may make disassembly of the channel/nozzle assembly very difficult for removal and replacement. Much more work will have to go into developing a good engineering solution for this.

The sodium column height should be varied to investigate the extent of completion of reaction, as determined by measurement of the effluent CO_2 and CO gas species, upon the sodium height. The CO_2 stagnation temperature should be varied to investigate heat exchanger failure at different locations between the hot and cold ends of the heat exchanger. The sodium column temperature should be varied to investigate differences between interactions in the inlet and outlet sodium header regions due to the different sodium temperatures as well as the differences in chemical reactions above and below the reaction threshold temperature of about 500 °C. Table 10 shows the test matrix for the sodium channel experiments.

4.6 Long term reaction product behavior in flowing sodium

The experiments discussed above focus on an examination of whether significant interaction of CO with sodium occurs on a short timescale as bubbles rise through the sodium column. It is possible that negligible interaction will be found in this short-term interaction mode. Assuming that CO might still react with sodium but on a significantly longer timescale, there is a need for experiments in which gas bubbles are injected into an isothermal flowing sodium loop through which they are transported over a long timescale. In particular, if the reaction is very slow, then it might be necessary to transport the gas through flowing sodium for days or weeks or even months. This implies that a loop capable of continuous operation for weeks or months is needed. This loop does not need to be large. The only requirements are that the tubing or piping size is large enough such that the bubbles are relatively small, and that the sodium velocity is high enough such that the bubbles are entrained into the sodium flow and remain entrained in the flow. Sodium flow can be established with an electromagnetic (EM) sodium pump and the loop can be completely horizontal (or nearly so) to reduce pumping head requirements. The loop should have an expansion volume connected to the rest of the loop by a vertical tubing or piping segment such that under flow conditions the gas bubbles will not separate from the sodium flow and rise to the free surface in the expansion volume.

The loop needs to incorporate the capability to withdraw a small volume of sodium from the flow at different times which can be subjected to measurement of the amount of gas present and the composition of gas. This is because it is expected that the number of CO molecules in the gas bubbles will decrease with increasing time. Determination of the timescale for CO interaction with sodium for different bubble sizes would be an important result. A plugging meter could also be used to detect the amount of sodium oxide Na_2O in the sodium which would be indirect evidence of the reaction of CO with sodium. An oxygen sensor should also be included in the loop but could be difficult to source since no known commercial vendor exists at this time.

It is also of interest to determine if solid sodium carbonate (Na_2CO_3) formed as a reaction product interacts with sodium forming sodium oxide and elemental carbon, and to determine the timescale for the reaction. Perhaps sodium carbonate could be added to the sodium in the loop and circulated. If the amount of dissolved oxygen in the sodium is measured to increase, then this could be evidence for the reaction of the carbonate with sodium. Thus, the loop would also need to be designed with a capability to add a solid powder such as sodium carbonate to the sodium without contaminating the sodium with oxygen at the same time.

Due to the formation and accumulation of sodium oxide that dissolves in the flowing sodium, it is necessary to replace the sodium with purified sodium containing only a small amount of dissolved oxygen from time to time. One approach is to add a cold trap branch circuit to the loop that can be operated to precipitate out and trap dissolved oxygen thereby purifying the same volume of sodium. However, it is possible for carbonates to be formed and accumulate in the sodium. Carbonates are not cold trapped out of sodium. Perhaps they can be filtered out by flowing a portion of the sodium through a suitable filtering system in a branch circuit.

A second approach that might be effective if the sodium inventory is sufficiently small is to simply replace the sodium with fresh pure sodium from time to time.

It might be possible to incorporate the long term interaction loop into the SNAKE facility. This approach might enable the use of certain SNAKE components or equipment that will exist following future improvements thereby saving some procurement costs. This is a long term vision for the SNAKE facility and is not expected to be implemented in the near term (i.e., not until after FY 2014) due to funding and schedule limitations. Table 10 shows a test matrix for the experiments with the small-scale isothermal flowing sodium loop.

5 Near-term detailed test matrix

The general test matrix described above will guide the development of detailed tests as the sodium-CO_2 interaction program continues. A more detailed near-term test matrix is developed here in order to describe and guide experiments that will be carried out for the remainder of FY 2013 into early FY 2014. Much of this testing will be characterized as shakedown testing in order to gradually verify proper sensor and supporting equipment operations. The first few experiments are expected to involve conservative conditions (i.e. low temperature, pressures, and sodium heights) to maximize safety. The shakedown tests are still designed to obtain useful data; however, data collection is not their primary purpose and would not be considered 'failures' should little data arise from the first few tests.

A summary of the target conditions for the first few experiments are listed in Table 12. All of these tests will be direct injection of CO_2 into a static sodium pool. For the first few tests, the sodium will be maintained at the lowest temperature it can safely be maintained at without any risk of freezing, around 160-180 ˚C. Over the course of several experiments the sodium temperature will gradually be increased, but it is not anticipated to reach the maximum facility operating temperature (510 ˚C) in the initial test series. The sodium column height will be kept low initially, and gradually increased, up to a maximum of approximately 80 cm. This height can be increased after enough experiments verify that gas-holdup is not pushing sodium high enough up to spill into the cover gas exhaust line. Pressure will be gradually increased from just over the critical point up to 20 MPa. Low pressure (sub-critical) CO_2 tests will also be carried out to add to the simulation verification database. Most tests will last approximately 30 minutes, or until steady state is reached on all primary instruments.

One test will be carried out to fully shakedown the new sodium level-detector (Test 4). The sodium level will gradually be increased and this will be verified on the detector. As part of this testing, a gas hold-up experiment will be run where CO_2 at varying pressures will be injected into the sodium column and the resulting height of the sodium will be measured. This experiment is useful to make the safety case for the maximum sodium height allowed, and also could be useful in providing novel data for gas hold-up in liquid metals.

A detailed CO monitor test will be run utilizing both the mass spectrometer and new dedicated thermal-acoustic CO gas monitor. Pure CO_2 gas and mixtures of argon, CO_2, and CO will be injected through the nozzle into an empty test vessel at various pressures. This

will simulate the time it takes for the gas mixtures to travel from the nozzle to the exhaust system where the gas monitors are. These types of tests act as baselines to compare with the sodium experiments that may generate some CO via the sodium-CO_2 reaction.

The first test listed was carried out in September 2013 and summarized in Gerardi et al. (2012b). Most of the remaining near-term tests listed in Table 12 do correspond to tests recommended in the general test matrix of Table 10. It is expected that slight deviations from what is listed in Table 12 will occur as the experimental reality on a given day and the results of previous tests are taken into account. These first tests will take place in FY 2013 and into FY 2014. It is also expected that most of the water-based tests discussed in the general test matrix will be carried out in this same time frame.

Table 12: Detailed near-term test matrix

CO_2 injection from micro-nozzle into open sodium pool						
Test #	**CO_2 stagnation pressure, MPa**	**CO_2 stagnation temperature, ˚C**	**Sodium column temperature, ˚C**	**Sodium column height, cm**	**Injected CO2 mass, kg**	**Test duration, min**
1	9	170	180	38.1	247	30
2	6	170	180	40	-	20
3	3	170	180	40	-	30
4	Sodium level detector testing and gas hold-up experiment			10-90	-	-
5	3-20	250	CO monitor testing without sodium in vessel		-	30
6	11	250	250	20	-	20
7	11	250	250	60	-	20
8	11	250	250	20	-	20
9	11	250	250	80	-	20
10	11	330	330	20	-	20
11	20	330	330	20	-	20
12	20	330	330	60	-	20
13	20	330	330	80	-	20

6 Summary

A first principles analysis and assessment of sodium (Na)-carbon dioxide (CO_2) interactions following the formation of a micro-leak inside of a compact diffusion-bonded sodium-to-CO_2 heat exchanger (HX) has been carried out. Based upon the results of the assessment, needs for fundamental experiments on sodium-CO_2 interactions have been identified, and for each type of experiment, a general test matrix has been formulated for testing in the ANL Na-CO_2 Interaction facility, SNAKE (S-CO_2 Na Kinetics Experiment). The detailed test matrix recognizes that with the ongoing incorporation of improvements to the facility in FY 2013, testing in FY 2013 and early FY 2014 may largely be characterized as shakedown testing. These improvements and the data obtained as experiments are carried out may result in experiments being added or removed from the test matrix in order to maximize understanding of the Na-CO_2 interactions. A near-term test matrix was also generated to summarize the target conditions for the first thirteen experiments.

References

1. M. Anderson, G. Mignot, and M. Corradini, "University of Wisconsin – Madison Experimental Investigation of Critical Flow of Supercritical Carbon Dioxide," Slides presented at the $SCCO_2$ Power Cycle Symposium 2009, RPI, Troy, NY, April 29-30, (2009).
2. R. M. Davies and Sir Geoffrey Taylor, F.R.S., "The Mechanics of Large Bubble Rising Through Extended Liquids and Through Liquids in Tubes," Proceedings of the Royal Society of London, Series A, Mathematical and Physical Sciences, Vol. 200, pp. 375-390, (1950).
3. J.H. Eoh, H.C. No, Y.H. Yoo, J.Y. Jeong, J.M Kim, S.O. Kim, "Wastage and Self-Plugging by a Potential CO_2 Ingress in a Supercritical CO_2 Power Conversion System of an SFR," J. Nuclear Science and Technology, Vol. 47(11), pp. 1023-1036, (2010).
4. M.T. Farmer, D.J. Kilsdonk, J.J. Sienicki, and C. Grandy, "Design of a Test Facility to Investigate Fundamental Na-CO_2 Interactions in Compact Heat Exchangers," ANL-GENIV-164, (2010).
5. J. Fink, L. Leibowitz, "Thermodynamic and Transport Properties of Sodium Liquid and Vapor," Argonne National Laboratory, ANL/RE-95/2, (1995).
6. C. Gerardi, M.T. Farmer, D.J. Kilsdonk, J.J. Sienicki, and C. Grandy, "Fundamental Na-CO_2 Interactions in Compact Heat Exchangers Experiment (SNAKE): FY 2011 Status Update," ANL-ARC-199, (2011).
7. C. Gerardi, M.T. Farmer, D.J. Kilsdonk, J.J. Sienicki, and C. Grandy, "Na-CO_2 Interactions Experiment (SNAKE): FY 2012 Update on Facility Assembly and Sodium Loading," ANL-ARC-230, (2012a).
8. C. Gerardi, M.T. Farmer, D.J. Kilsdonk, R. Aeschlimann, J.J. Sienicki, and C. Grandy, "Report on the Initial Fundamental Sodium-CO2 Interaction Experiment," ANL-ARC-251, (2012b).
9. L. Gicquel, C. Latgé, and N. Simon, "Supercritical CO_2 Brayton Cycle Coupled with a Sodium Fast Reactor: Na/CO_2 Interaction Experiments and Modeling," Paper 10215, 2010 International Congress on Advances in Nuclear Power Plants (ICAPP '10), San Diego, CA, USA, June 13-17, (2010).
10. L. Gicquel, C. Latgé, and N. Simon, Ph. Hobbes, A. Soboni, J.C. Buvat, J.L. Gustin, "Brayton Cycle with SC-CO_2: Investigations of Sodium-Carbon Dioxide Interactions," Slides from Meeting with A. Moisseytsev (ANL), April 27-29, (2011).
11. V. Gnielinski, "Neue Gleichungen für den Wärme- und den Stoffübergang in turbulent durchströmten Rohren and Kanälen," Forsch. Ing.-Wes., Vol. 41, No. 1, pp. 8-16, (1975).
12. F.P. Incropera, and D.P. DeWitt, *Fundamentals of Heat and Mass Transfer*, 5th Ed., (2002).
13. P.-S. Lee and S. V. Garimella, "Thermally Developing Flow and Heat Transfer in Rectangular Microchannels of Different Aspect Ratios," Int. J. Heat Mass Transfer, Vol 49, pp 3060-3067, (2006).

14. A. Moisseytsev and J.J. Sienicki, "Development of a Plant Dynamics Computer Code for Analysis of a Supercritical Carbon Dioxide Brayton Cycle Energy Converter Coupled to a Natural Circulation Lead-Cooled Fast Reactor," ANL-06/27, Argonne National Laboratory, July (2006).
15. A. Moisseytsev, J. J. Sienicki, D. H. Cho, and M. R. Thomas, "Comparison of Heat Exchanger Modeling with Data from CO2-to-CO2 Printed Circuit Heat Exchanger Performance Tests," Paper 10123, Proceedings of ICAPP '10, San Diego, CA, June 13-17, (2010).
16. NIST Thermophysical Properties of Fluid Systems, http://webbook.nist.gov/chemistry/fluid/, Accessed April (2013).
17. W.C. Reynolds, Thermodynamic Properties in SI, Graphs, Tables and Computational Equations for Forty Substances, Department of Mechanical Engineering, Stanford University, Stanford, 1979.
18. D. Rodrigue, "Generalized Correlation for Bubble Motion," AIChE Journal, Vol. 47, No. 1, pp. 39-44, January (2001).
19. F. Rouillard, S. Bouhieda, G. Moine, J. Ruiz, and P. Venditti, "Corrosion Study of Steels in CO_2 Influence of Environmental Parameters," Generation IV International Forum Sodium-Cooled Fast Reactor Component Design and Balance of Plant Project Management Board Meeting, Tsuruga, Japan, February 14-17, (2012).
20. D. Southall, "Diffusion Bonding in Compact Heat Exchanger," Proceedings of SCO_2 Power Cycle Symposium 2009, Rensselaer Polytechnic Institute, Troy, NY, April 29-30, (2009).
21. R. Span, and W. Wagner, "A New Equation of State for Carbon Dioxide Covering the Fluid Region from the Triple-Point Temperature to 1100K at Pressure up to 800 MPa", J. Phys. Chem Ref. Data, Vol. 25(6), pp. 1509-1596, (1996).
22. N.E. Todreas, and M.S. Kazimi, *Nuclear Systems I: Thermal Hydraulic Fundamentals*, Taylor & Francis, (1990).


Argonne
NATIONAL LABORATORY

Nuclear Engineering Division
Argonne National Laboratory
9700 South Cass Avenue
Argonne, IL 60439

www.anl.gov

Argonne National Laboratory is a U.S. Department of Energy
laboratory managed by UChicago Argonne, LLC